SCALING OF TURBULENT MIXED CONVECTION UNDER HIGH PRESSURE

Andreas Westhoff, Nina Grabinski, Johannes Bosbach and Claus Wagner
German Aerospace Centre Göttingen (DLR)
Institute of Aerodynamics and Flow Technology
Bunsenstr. 10, D-37073 Göttingen, Germany
andreas.westhoff@dlr.de

Andre Thess
Department of Mechanical Engineering,
University of Technology Ilmenau,
P.O. Box 100565, D-98684 Ilmenau, Germany
andre.thess@tu-ilmenau.de

ABSTRACT

Measurement of turbulent mixed convection at reduced model size by aerodynamic scaling is a promising approach to simplify the investigation of many technical configurations and offers the potential to make large scale flows accessible on a laboratory scale. First results of an experimental study of turbulent mixed convection in a generic convection cell at ambient and high pressure are reported.

The aim of these measurements is to prove the possibility of scaling mixed convection by varying fluid pressure and inflow velocity. We present and discuss results for mixed and forced convection obtained with air as working fluid ($Pr \approx 0.7$) at ambient pressure for $Gr = 3.52 \cdot 10^6$, $Re = 1.1 \cdot 10^3$ and thus $Ar = 1.81$ and at 10 bar with $Gr = 3.51 \cdot 10^8$, $Re = 1.1 \cdot 10^4$ and thus $Ar = 1.83$. The scaling theory, which allows to scale the cell, is presented as well as the PIV set up used for measurement at high pressure conditions in the High Pressure Wind Tunnel of Göttingen (HDG) and the convection cell.

At elevated fluid pressure a significant increase of the velocity fluctuations was observed. Furthermore for mixed convection a transition of a stable 2D flow into an instationary 3D flow has been found.

INTRODUCTION

The superposition of forced and free convection is called mixed convection. It is characterized by the Archimedes number Ar

$$Ar = \frac{\sqrt{Gr}}{Re}, \tag{1}$$

i. e. the ratio of buoyancy and inertia forces, the Reynolds number Re and the Prandtl number Pr. Gr denotes the Grashof number and reflects the impact of buoyancy on the flow. For very small Ar the flow is governed by inertia forces, while at very high Ar buoyancy forces dominate. In the intermediate region of Ar the flow field depends on both, buoyancy and inertia forces. This regime is referred to as mixed convection which occurs in many technical applications like e.g. heat exchangers (Sillekens et al. (1998)), air conditioning of passenger compartments (Bosbach et al. (2006)) or climatisation of buildings (Linden (1999)). Moreover, mixed convection is an often occurring phenomenon in geology and meteorology. Since many of these flow situations involve large scales, acquiring such flows experimentally at full scale can be difficult. As a consequence a measurement method which allows for investigation of large scale mixed convection at reduced model size is highly desirable. The approach of our experiment is to reduce the spatial dimensions of such configurations to scales which are experimentally accessible by increasing the fluid pressure and the inflow velocity and thus keeping Gr, Re, Pr and thereby Ar constant.

Several studies exist, which consider mixed convection in different configurations, using various measurement techniques and parameter ranges. A configuration often chosen for such investigations is mixed convection between two horizontal plates cooled from above and heated from below. Polyakov et al. (1988) studied mixed convection at $3530 < Gr < 1.18 \cdot 10^4$ and $15 < Re < 150$ with Laser-Doppler anemometry. You et al. (2002) conducted numeric simulations for this configuration. Baskaya et al. (2005) studied the impact of buoyancy forces on the local Nusselt number for $241 < Re < 980$ and $9.53 \cdot 10^5 < Gr < 1.53 \cdot 10^7$ in a horizontal channel, which was equipped with an array of discrete heat sources at the bottom. Costa (1999) investigated mixed convection of a hot air jet with two-component Laser-Doppler anemometry. Other studies, which deal with flows in rectangular cells were considered for different boundary conditions and aspect ratios by Shankar et al. (2002),for a vertical rectangular duct with a Gr/Re ratio of up to 600 and several aspect ratios by Barletta et al. (2003). Closely related to our study are measurements of Rayleigh-Bérnard convection at high Rayleigh numbers using different pressurized gases as fluid. For example, Fleischer and Goldstein (2002) worked with Rayleigh numbers up to $Ra = 1.7 \cdot 10^{12}$, whereas Niemela (2006) examined the scaling of Nusselt number with Rayleigh number for Ra up to 10^{17}. However, to our knowledge, measurements of mixed convection at high fluid pressure, particularly by means of PIV, have not been performed so far. At the German Aerospace Centre in Göttingen a modularly designed convection cell was developed allowing to study mixed convection in a range of $600 < Re < 3 \cdot 10^6$, $5 \cdot 10^5 < Gr < 5 \cdot 10^{10}$. In order to cover this range the cell can be operated within a pressure range of $1 < p < 100$ bar. The aim is to apply PIV at high pressure in order to study the influence of buoyancy on the forced convection at high Grashof and Reynolds numbers considering the concept of a scaling theory.

SCALING THEORY

Mixed convection in a given geometry is characterised by

the non dimensional parameters

$$Gr = \frac{g\alpha\Delta T H^3}{\nu^2}, \tag{2}$$

$$Re = \frac{UL}{\nu} \tag{3}$$

and

$$Pr = \frac{\nu}{\kappa}, \tag{4}$$

where g denotes the gravitational acceleration, H the height of the cell, $\alpha = -1/\rho(\partial\rho/\partial T)$ the thermal expansion coefficient, ν the kinematic viscosity, κ the thermal diffusivity, U the inlet velocity, ρ the density and L the characteristic length scale of the system. Often one would like to study the flow with the same nondimensional parameters but in a geometry whose size $\hat{H}$ is by a factor s smaller than its original size, i.e. $\hat{H} = s_H \cdot H$. Scaling theory tells us how one has to scale velocity, viscosity, thermal diffusivity, and the thermal expansion coefficient in order to accomplish this task. Assuming that the thermal expansion coefficient is independent of pressure for our working fluid air one can readily verify that the scaling coefficients for the mentioned quantities are related to s by the equations

$$Gr = \frac{g\alpha\Delta T (s_H H)^3}{s_\nu^2 \nu^2}, \tag{5}$$

$$Re = \frac{s_U U s_L L}{s_\nu \nu} \tag{6}$$

and

$$Pr = \frac{s_\nu \nu}{s_\kappa \kappa}. \tag{7}$$

The corresponding scaling factors are denoted as s_i. Under the constraint of geometrical similarity, i.e. $s_L = s_H$, we obtain the two equations

$$s_\nu = (s_H)^{\frac{3}{2}} \text{ and } s_U = (s_H)^{\frac{1}{2}} \tag{8}$$

Scaling of the system by a factor s_H for the height of the container yields the scaling factors for kinematic viscosity s_ν and the inflow velocity s_U. Since μ, the dynamic viscosity, is unaffected by the pressure in the regime of $1 < p < 20$ bar, the kinematic viscosity can be controlled via the density ρ, which in turn depends on the pressure p linearly for air. This allows to compare a large scale system to a downscaled system by increasing the pressure and adjusting the inflow velocity.

EXPERIMENTAL SETUP

High Pressure Wind Tunnel

The measurements were performed in the High Pressure Wind Tunnel Göttingen (HDG), which is a Göttingen-type closed circuit low speed wind tunnel that can be pressurized up to 100 bar (figure 1). The velocity is adjustable between 3.5 and 35 m/s in the total range of pressure. At a temperature of 300 K with the standard reference length definition of 0.06 m, the Reynolds number can be varied up to $1.2 \cdot 10^7$. The test section has a height of 0.6 m, a width of 0.6 m and a length of 1 m.

The function of the HDG in our experiments is threefold. First it allows to adjust the fluid pressure, second it provides the inflow of our convection cell, and finally it supplies cooling to the cell ceiling.

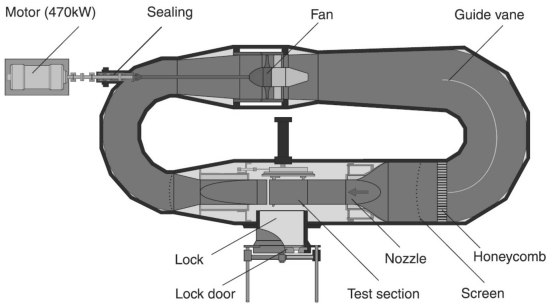

Figure 1: Sketch of the High Pressure Wind Tunnel Göttingen (HDG).

Convection cell

Our convection cell (see figure 2) consists of a cuboidal container with a quadratic cross section, an air inlet at the top and an air outlet at the bottom. The cell has a width of 0.1 m, a height of 0.1 m and a length of 0.5 m. In- and outlet are located at the same side of the cell. Both, air in- and outlet, span the whole length of the cell and are constituted by rectangular channels with a channel height of 5 mm and a length of 300 mm for the inlet and a channel height of 3 mm and a length of 120 mm for the outlet The inlet channel is equipped with an additional fence in order to further homogenize the inflow. All side walls are thermally insulated by a layer system with an insulating sheath of 7 mm air between two layers of transparent windows in order to accomplish almost adiabatic boundary conditions while maintaining the optical accessibility of the cell.

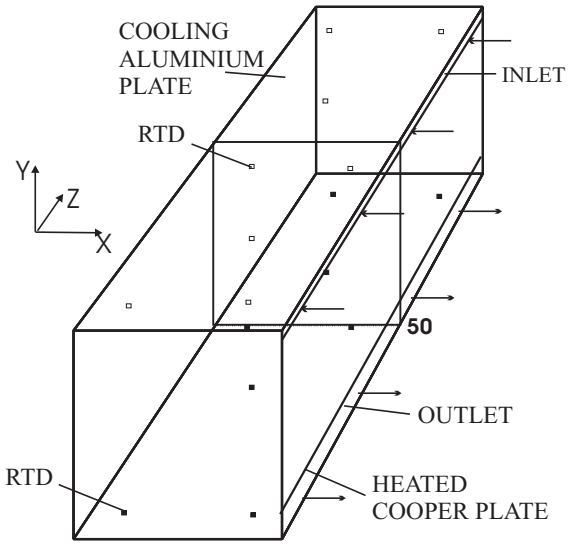

Figure 2: Sketch of the convection cell with heated copper plate at the bottom, cooling aluminium plate at the top, inlet, outlet and embedded RTDs (black in heating, white in cooling plate).

The floor of the container is equipped with a heated copper plate and the ceiling with an aluminium heat exchanger. Cooling is realized by cooling fins, which provide thermal coupling between the cooling plate and the air in the wind tunnel.

Resistance Temperature Detectors (RTDs) are embedded in the cooling and heating plate (see figure 2) in order to monitor the temperatures of our cell. Further the in- and

outflow temperature are recorded with RTDs. Additional to the temperature the dynamic pressure at the outlet was measured with a Pitot-tube in combination with a static pressure probe in order to determine the average inflow velocity $\hat{v}_{\mathrm{in}}$.

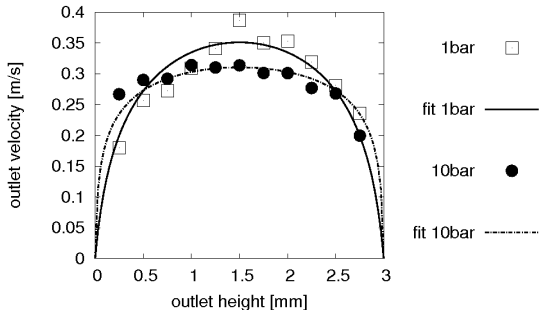

Figure 3: Outlet velocity profile for mixed convection at $Ar \approx 1.8$ at ambient pressure and 10 bar.

The dynamic pressure was scanned in steps of 0.25 mm of the outlet height. By means of equation 9 a least squares fit of the outlet velocity profile as determined from the time averaged dynamic pressure measurements was calculated (see figure 3):

$$v(y) = v_\tau \frac{1}{\kappa} \ln\left(1 - Re_\tau \frac{\kappa}{2}\left(1 - \left(\frac{y}{H_{\mathrm{out}}/2}\right)\right)\right), \quad (9)$$

where Re_τ the Re based on the friction velocity v_τ and κ the von Kármán constant. Averaging of the model function (equation 3) over the channel height yields the average outlet velocity $\hat{v}_{\mathrm{out}}$. Due to mass conservation the average inlet velocity amounts to $\hat{v}_{\mathrm{in}} = \frac{3}{5}\hat{v}_{\mathrm{out}}$. For both cases $\hat{v}_{\mathrm{in}}$ was determined to be 0.17 m/s.

With this configuration we are able to generate mixed convection under well defined conditions and adjustable fluid pressure.

Particle Image Velocimetry set up

Particle Image Velocimetry (PIV) has been applied in order to measure mixed convection in our cell. The PIV system consists of a double oscillator quality switched Nd:YAG laser, a light sheet optics and a Peltier-cooled charge coupled device (CCD) camera (1376x1040 spatial resolution at 12 bit grayscale), which is placed in front of the convection cell. The light sheet is injected into the cell from the opposite side of the air inlet According to the optical set-up only the velocity components in the light sheet plane were detected (2C-2D PIV). As seeding Matroxid (Al_2O_3) particles with diameters between 3 and 5 μm were used. They were injected into the flow by a fluidized-bed seeding generator (a detailed description can be found in Willert and Jarius (2002)).

Measurement procedure

Forced and mixed convection have been investigated for various pressure levels. The measurements presented here were conducted at ambient pressure and at 10 bar in the cross section at 50 percent of the cell length ($Z/2$). As already mentioned air was used as working fluid. For forced and mixed convection the Re number, based on the height of the cell as characteristic length and the average inflow velocity $\hat{v}_{\mathrm{in}} = 0.17$ m/s amounts to about $Re = 1.1 \cdot 10^3$ at 1 bar and to $Re = 1.1 \cdot 10^4$ at 10 bar fluid pressure. A temperature difference of about 30 K between heating and cooling plate resulted in a Grashof number of $Gr = 3.51 \cdot 10^6$ at 1 bar and $Gr = 3.52 \cdot 10^8$ at 10 bar. As a consequence the Archimedes number for mixed convection amounted to $Ar = 1.8$ for both cases of mixed convection (see also table 1). Therefore we would like to mention that the lateral temperature deviations on the heating plate as measured with the RTDs are less than 0.2 K and at the heating plate and less than 0.01 K on the cooling plate. The velocity fields in the measurement plane were recorded in 3 series of 160 double images at a repetition rate of 2.5 Hz and 500 double images at a repetition rate of 0.5 Hz. From these 980 instantaneous 2C-2D velocity fields the average as well as the root mean square of the deviations from the average (RMS) has been calculated. Along with the in-plane velocity vectors the 2C velocity magnitude $W = \sqrt{U^2 + V^2}$ of the flow field has been evaluated. The x- and y-coordinates are made dimensionless by division with the height of the cell. The z-coordinate is made dimensionless by division with the length of the cell. The velocity of the flow field is depicted using vectors with the length of the in-plane velocity magnitude. Both RMS values and the velocity magnitude were made dimensionless with the averaged inflow velocity $\hat{v}_{\mathrm{in}} = 0.17$ m/s.

Table 1: Measurement conditions for forced and mixed convection at 1 and 10 bar.

No.	Gr	Re	Ar	ΔT [K]	ρ [kg/m^3]
1.	-	1190	-	-	1.28
2.	$3.52 \cdot 10^6$	1110	1.81	30.1	1.23
3.	-	11100	-	-	11.9
4.	$3.51 \cdot 10^8$	10300	1.83	30.4	11.6

RESULTS AND DISCUSSIONS

For the sake of visibility in figure 4,6,8,10,12 and 13 only every second vector is plotted in each direction in the vector plots. The RMS values are presented as contour lines with levels between 0 and 10. The reference vector (shown at left upper corner of the time-averaged velocity fields) is scaled to $\hat{v}_{\mathrm{in}}$.

Averaged velocity field

Figure 4 depicts the time averaged velocity field for forced convection at ambient pressure (case No. 1). Clearly, the jet of incoming air from the inlet (upper right corner) can be detected. The flow follows the ceiling and detaches at $X \approx 0.4$ and descend at the left sidewall. At $Y \approx 0.3$ it detaches again, flows parallel to the bottom plate and splits in two parts: One follows the right sidewall into the direction of the inlet and the other part leaves the cell through the outlet (lower right corner). As result a mean wind rotating in opposite clockwise direction with a core located in the centre of the cell develops.

By contrast the time averaged velocity field of mixed convection (figure 6, case No. 2) reveals a jet attaching to the right side wall close to the inlet The jet splits at the bottom in two parts: One part leaves the cell through the outlet and the other part follows the mean wind. The mean wind in this case is also a role-structure with a core located near the centre of the cell but as opposed to forced convection

and due to the action of buoyancy it is rotating clockwise.

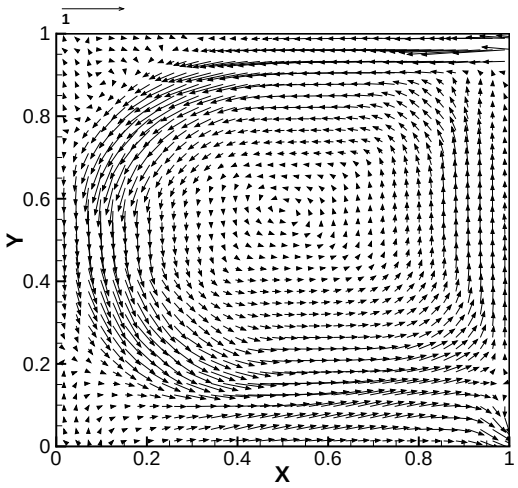

Figure 4: Time-averaged in-plane velocity fields at $Z/2$ for forced convection at ambient pressure with $Re = 1190$.

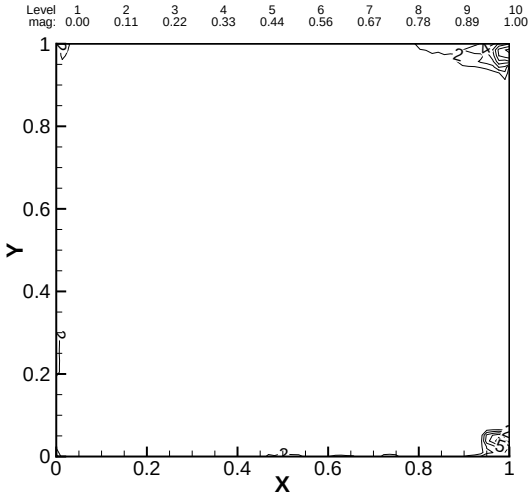

Figure 5: RMS values of the velocity fluctuations corresponding to the results of figure 4.

The averaged velocity fields of forced and mixed convection at a pressure of 10 bar are shown in figures 8 (case No. 3) and 10 (case No. 4). For forced convection at 10 bar fluid pressure (case No. 3) the mean wind is almost comparable to the flow for forced convection at ambient pressure (case No. 1). The main differences concern the incoming air jet which is detaching a bit later at $Y \approx 0.3$, the centre of mean wind (role-structure) which is shifted lightly to the lower right corner, the boundary layer which is thinner, and the role thickness which is increased.

In contrast to forced convection (case No. 3) the averaged velocity field of mixed convection at 10 bar (case No. 4) shows a totally different behaviour. The flow in the measurement plane is dominated by a rising flow, indicating a three dimensional break down of the mean wind. The incoming air jet follows the ceiling to the left sidewall and flows downward at the left sidewall where it hits on the rising air at $Y \approx 0.5$, resulting in an out of plane evasion. A stream at the bottom of the cell which comes out of plane at the lower left corner leaves the cell through the outlet

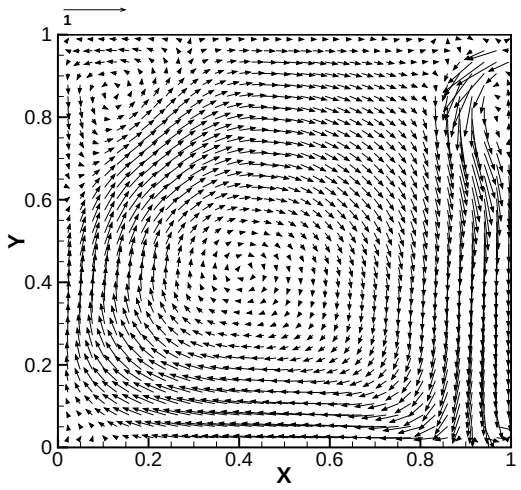

Figure 6: Time-averaged in-plane velocity fields at $Z/2$ for mixed convection at ambient pressure with $Gr = 3.51 \cdot 10^6$, $Re = 1110$ and thus $Ar = 1.81$.

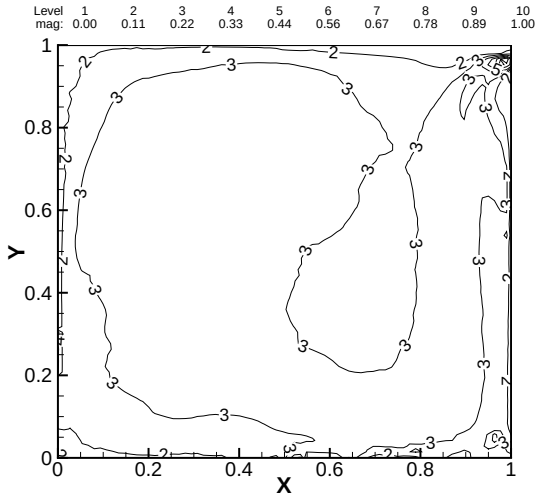

Figure 7: RMS values of the velocity fluctuations corresponding to the results of figure 6.

Statistical quantities of the velocity maps

Figure 5, 7, 9 and 11 depict the maps of the RMS values of forced and mixed convection at 1 bar and 10 bar, respectively. For the forced convection at ambient pressure (figure 5, case No. 1) the velocity fluctuations are less than 0.11 in the hole cross-section, except for the regions close to the in- and outlet This reveals a rather stationary behaviour of the mean wind. The increased RMS values in the region of in- and outlet are caused partially by background reflections in the PIV measurement.

By contrast at 10 bar (figure 9, case No. 3) the RMS map clearly reflects the influence of the higher pressure on the flow. A dramatical increase of the velocity fluctuations, particularly in the region of the vortex at the upper left corner and in the region of the incoming jet is caused by the change of Re. In the region of the rotating mean wind the RMS values are rather low.

The contour map of the RMS values for the case of mixed convection under ambient pressure (figure 7, case No. 2) clearly shows the influence of the buoyancy forces on the velocity fluctuations. It can be recognised that the RMS values are drastically increased as compared to forced convection

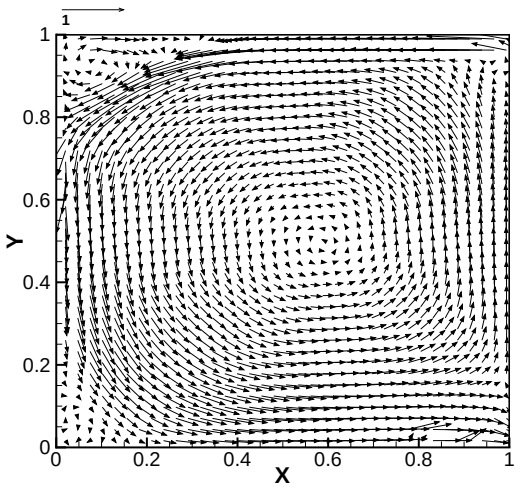

Figure 8: Time-averaged in-plane velocity fields at ZS/2 for forced convection at a pressure of 10 bar with $Re = 1.11{\cdot}10^4$.

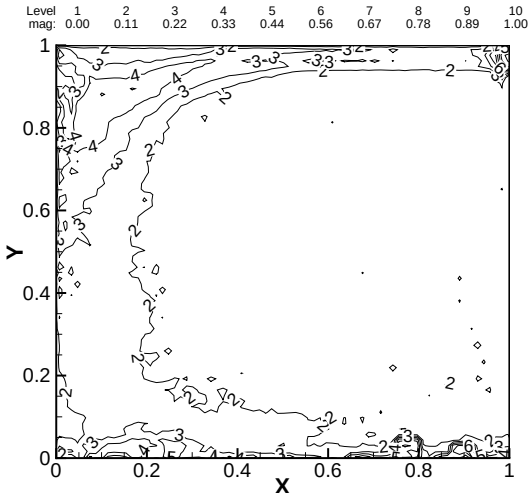

Figure 9: RMS values of the velocity fluctuations corresponding to the results of figure 8.

(case No. 1) over the hole cross-section. The velocity fluctuations in the wall region amount to between 0.11 and 0.22 and raise up to 0.33 in the major part of the centre region.

For the case of mixed convection at 10 bar (figure 11, case No. 4) an increase of the velocity fluctuations as compared to the case of forced convection (case No. 3) can be identified. The velocity fluctuations in the wall region are increased up to 0.33 and in the centre region up to 0.44. As compared to mixed convection at ambient pressure (case No. 2) the RMS values are increased by 10 percent in average over the whole measurement plane. The region of the largest RMS values develops where the uprising air hits the incoming air jet

Effects of pressure increase

By increasing the pressure from 1 to 10 bar and keeping ΔT, the inflow velocity and thus Ar constant we the characteristic height H was scaled by a factor of 4.6. As already pointed out this leads to a totally different time averaged flow field in the cross-section at Z/2 for the case of mixed convection. Further the velocity field of mixed convection changed from almost 2D to 3D flow.

The instantaneous velocity fields for the case of mixed

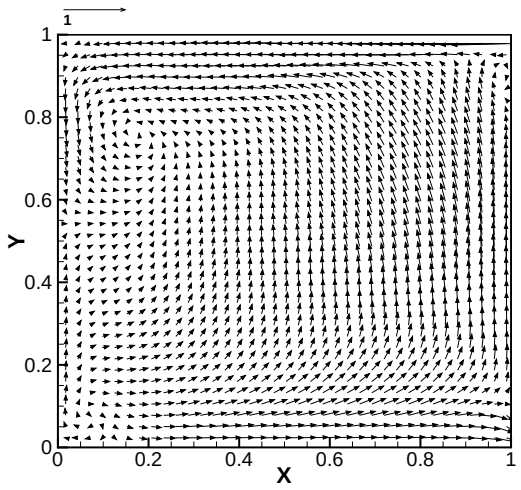

Figure 10: Time-averaged in-plane velocity fields at $Z/2$ for mixed convection at ambient pressure with $Gr = 3.51 \cdot 10^8$, $Re = 1.03 \cdot 10^4$ and thus $Ar = 1.83$.

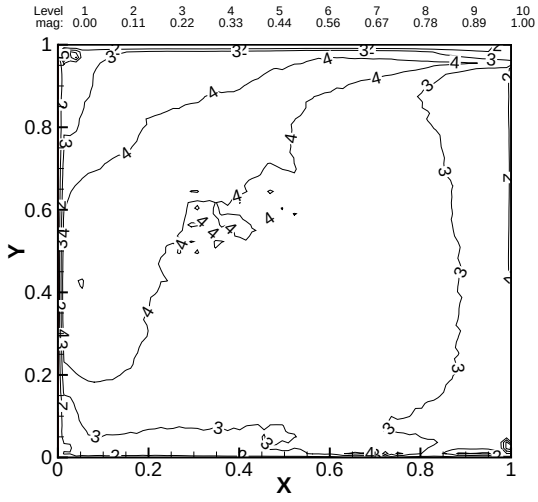

Figure 11: RMS values of the velocity fluctuations corresponding to the results of figure 10.

convection at ambient pressure and 10 bar (figure 12, case No. 2) and 1 bar (figure 13, case No. 4)) clearly reflect the impact of the pressure increase. While for case No. 2 the structure of the main flow can be still detected, these structures break down into smaller structures due to the pressure increase.

It should be noted as well, that the temperature difference between in- and outflow, ΔT_{out}, decreases from 11 K to 8 K upon the increase of the fluid pressure. This difference might be caused by changes of the mixing behaviour due to variation of the main flow structure as well as changes of shear stresses and heat transition between fluid and cell.

SUMMARY AND CONCLUSION

Forced and mixed convection have been investigated in a rectangular convection cell at ambient pressure and 10 bar by Particle Image Velocimetry. By increasing the fluid pressure scaling of our model by a factor of 4.6 has been achieved.

As expected, the elevated fluid pressure causes a significant increase of the velocity fluctuations, especially for the

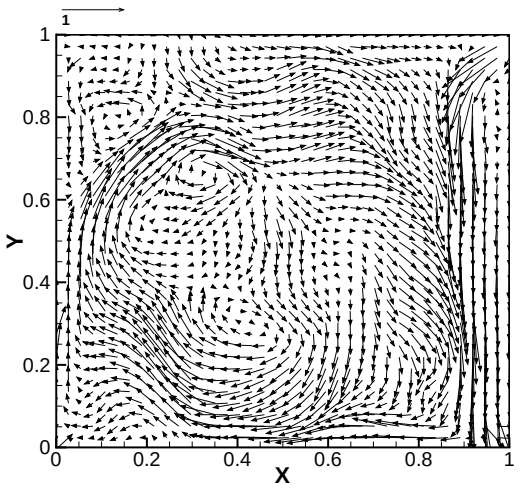

Figure 12: Instantaneous velocity field for mixed convection at ambient pressure.

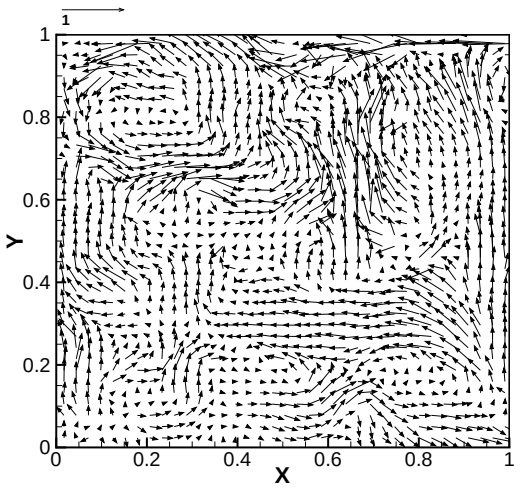

Figure 13: Instantaneous velocity field for mixed convection at 10 bar.

case of forced convection due to scaling of Re by a factor of 10. Further for mixed convection a transition of the rather stable 2D mean wind into an instationary 3D flow was caused by the model scaling.

Finally we have demonstrated PIV measurements under high pressure up to 10 bar. By a further increase of the fluid pressure up to 100 bar our method offers the potential of scaling by even a factor of up to 20.

ACKNOWLEDGMENT

We thank Dr. C. Willert and the DLR department Triebwerksmesstechnik (AT-TM) for providing the fluidized-bed seeding generator and M. Rippel for his support during the mearurements in the HDG.

REFERENCES

Sillekens, J. J. M., Rindt, C. C. M., and Van Steenhoven, A. A., 1998, "Developing Mixed Convection in a Coiled Heat Exchanger", Int. Journal of Heat and Mass Transfer, vol. 41, pp. 61-72.

Bosbach, J., Kühn M., Wagner C., Raffel M., Resagk C., du Puits R., and Thess A., 2006, "Large-scale particle image velocimetry of natural and mixed convection", 13th Int. Symp. on Applications of Laser Techniques to Fluid Mechanics, Lisbon, Portugal.

Barletta, A., Di Schio, E.R., and Zanchini, E., 2003, "Combined forced and free flow in a vertival rectangular duct with prescribed wall heat flux", Int. Journal of Heat and Mass Transfer, vol. 24, pp. 874-887

Linden, P. F., 1999, "The Fluid Mechanics of Natural Ventilation", 1999, Annu. Rev. Fluid Mech., vol. 31, pp. 201-238.

Polyakov, A. F., Shindin S. A., 1988, "Development of turbulent heat transfer over the length of vertical tubes in the presence of mixed air convection", Int. J. Heat Mass Transfer, vol. 31, pp.987-992.

You, J., Yoo, J. Y., and Choi, H., 2002, "Direct numerical simulation of heated vertical air flow in fully developed turbulent mixed convection", Int. Journal of Heat and Mass Transfer, vol. 46, pp.1613-1627.

Baskaya, S., Erturhan, U., and Sivrioglu, M., 2005, "Experimental investigation of mixed convection from an array of discrete heat sources at the bottom of a horizontal channel", Heat Mass Transfer, vol. 42, pp.56-63.

Costa, J. J., Oliveira, L. A., and Blay, D., 1999, "Test of several versions for the $\kappa - \epsilon$ turbulence modeling of internal mixed convection flows", Int. Journal of Heat and Mass Transfer, vol. 42, pp. 4391-4409.

Shankar, P.N., Meleshko, V. V., and Nikiforovich, E. I., 2002, "Slow mixed convection in rectangular containers", Journal Fluid Mech., vol. 471, pp. 203-217.

Fleischer, A.S. and Goldstein, R.J., (2002), "High Rayleigh number convection of pressurized gases in a horizontal enclosure", Journal Fluid Mech., vol. 469, pp. 1-12.

Niemela, J. J., Skrebek, L., and Donnelly, R., (2006), Turbulent convection at very high rayleigh numbers", Nature, vol. 404, pp. 837-840.

Willert C., and Jarius M., 2002, "Planar flow field measurements in atmospheric and pressurized combustion chambers", Experiments in Fluids, vol. 33, pp. 931-939